Chinese Chemical Letters 36 (2025) 110193

Contents lists available at ScienceDirect

Chinese Chemical Letters

journal homepage: www.elsevier.com/locate/cclet

Construction of a black phosphorous-based noncovalent multiple nanosupramolecular assembly for synergistic targeted photothermal and chemodynamic therapy

Yu-Hui Zhang[a,c,1,*], Ye Tian[a,1], Xianliang Sheng[a,*], Chen-Shuang Liu[a], Lu-Qiang Wei[a], Jie Wang[a], Yong Chen[b,*]

[a] College of Science & College of Material Science and Art Design, Inner Mongolia Agricultural University, Hohhot 010018, China
[b] College of Chemistry, State Key Laboratory of Elemento-Organic Chemistry, Nankai University, Tianjin 300071, China
[c] Inner Mongolia Key Laboratory of Soil Quality and Nutrient Resource & Key Laboratory of Agricultural Ecological Security and Green Development at Universities of Inner Mongolia Autonomous, Hohhot 010018, China

ARTICLE INFO

Article history:
Received 30 March 2024
Revised 20 June 2024
Accepted 28 June 2024
Available online 28 June 2024

Keywords:
Black phosphorus
Host-guest interaction
Cyclodextrin
Polysaccharide supramolecular assembly

ABSTRACT

Black phosphorus (BP), as a rising star of 2D nanomaterials has drawn considerable attention in cancer therapy. However, the poor stability under ambient conditions limits their practical applications. Herein, a multiple supramolecular assembly composed of adamantane-modified hyaluronic acid (HAADA), ferrocene-modified cinnamaldehyde (Fc-CA), guanidinium-functionalized β-cyclodextrin (Guano-CD), and black phosphorus (BP) nanosheets was successfully fabricated through cooperative host-guest and electrostatic interactions. Owing to the cooperative contribution of these building blocks, the obtained supramolecular assembly simultaneously possesses multiple functions including excellent stability, good biocompatibility and targeting property, and a high inhibition effect toward cancer cells. We believe that this work might provide new insights into designing a new generation of cancer theranostic protocols for potential clinical applications.

Recently, black phosphorus (BP) nanosheets have become a rising star in biomedical applications [1-4]. Compared with other 2D materials, BP possesses excellent biocompatibility and good biodegradability because BP can degrade into harmless phosphate in physiological environments which is a vital element for living organisms [5-8]. However, the practical applications of BP were severely impeded as its rapid degradation upon exposure to ambient conditions [9-11]. Therefore, several approaches were developed to stabilize BP and fabricate BP-based delivery systems for synergistic cancer therapy. For instance, Deng and co-workers reported a strategy of using a platinum-based anticancer drug to stabilize BP, which evades the potential clinical application risks concurrently constructing a stable BP-based drug delivery system for combined photothermal therapy (PTT) and chemo therapy [12]. Zhang and co-workers utilize the inherent Cu^{2+}-capturing ability of BP to develop BP@Cu nanostructures. The incorporation of Cu^{2+} not only enhances the photothermal performance/stability, but also provides the proof-of-concept application of BP-based materials in positron emission tomography (PET)-guided, chemodynamic therapy (CDT)-enhanced combination cancer therapy [13]. Mei and co-workers developed a simple polydopamine modification method to enhance the stability and photothermal performance of bare BP nanosheets [14]. BP undergoes continuous oxidation and degradation because its lone pair electrons is very reactive with oxygen to form P_xO_y. The platinum-based anticancer drug and Cu^{2+} could stabilize BP mainly utilizing coordination interaction to stabilize the lone pair electrons of BP, resulting in the formation of P^{5+} species and inhibiting the oxidation of BP. Polydopamine could stabilize BP due to the coating effect, and the polydopamine coating could adhere to the surface of BP and isolate the internal BP from external oxygen and water, which could effectively prevent the degradation of BP.

Although some strategies have been employed and exhibited enhanced stability and photothermal performance, there still exist several challenges in fabricating BP-based synergistic delivery systems such as the increased toxicity, the complicated construction procedure, and lack of specificity, which hinder the further advance [15,16]. To this end, supramolecular chemistry provides a promising and facile strategy to construct smart delivery systems

* Corresponding authors.
E-mail addresses: yh_zhangyh@126.com (Y.-H. Zhang), shengxl@iccas.ac.cn (X. Sheng), chenyong@nankai.edu.cn (Y. Chen).
[1] These authors contributed equally to this work.

https://doi.org/10.1016/j.cclet.2024.110193
1001-8417/

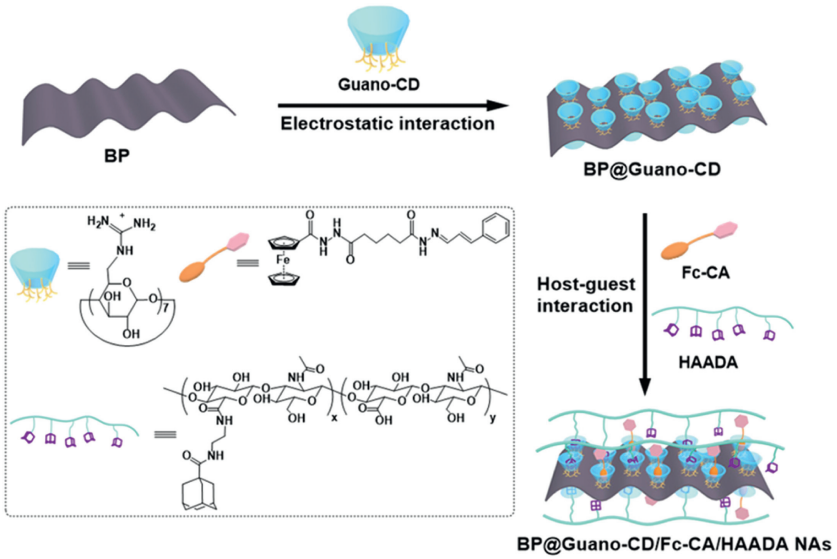

Scheme 1. Construction of the multiple nanosupramolecular assembly NAs from BP, Guano-CD, Fc-CA, and HAADA.

to overcome these limitations [17,18], where they utilize noncovalent interactions such as host-guest interactions [19,20], electrostatic interactions [21-23], hydrogen bonding [24,25], π–π stacking [26], and van der Waals interactions [27]. In this regard, the incorporation of supramolecular strategy and BP into a self-assembled smart delivery system may confer several practical superiorities in pharmacotherapy [28]. First, as compared with covalent assemblies, multicomponent supramolecular assemblies could be constructed by mixing the building blocks in solution with the assistance of multivalent intermolecular noncovalent interaction, which could avoid the multiple synthesis steps and a complicated purification process [29,30]. Moreover, the noncovalent interactions, especially the host–guest interactions could be adjusted by external stimuli, such as redox [31,32], temperature [33], pH [34,35], enzyme [36], and light [37], which could be utilized for fabrication of stimuli responsive supramolecular assembly and endow the convenient dissociation. The representative macrocycles, such as cyclodextrin (CD) that is water-soluble, nontoxic, and possesses a hydrophobic cavity, have become a focus of interest for the construction of biocompatible assemblies [38-40]. In addition to the abovementioned advantages along with the water solubility, biocompatibility and targeting ability could be concurrently enhanced in the obtained supramolecular assembly, which endows the supramolecular systems widely utilized in the biological field [41-45].

Herein, a supramolecular noncovalent strategy was used to construct an integrated multiple systems by a supramolecular surface modification of BP with guanidinium functionalized β-cyclodextrin (Guano-CD) which contains a guanidinium moiety as a binding group and a β-cyclodextrin cavity for further functionalization. Taking advantage of the two-step synergistic noncovalent modification process, *i.e.*, the electrostatic interaction between BP nanosheets and the guanidinium group, the supramolecular complexation of β-CD cavity with the Fc group of ferrocene-modified cinnamaldehyde (Fc-CA) and ADA group of adamantane-modified hyaluronic acid (HAADA) [46-48], the multiple nanosupramolecular assembly BP@Guano-CD/Fc-CA/HAADA (NAs) was successfully fabricated (Scheme 1). There are some inherent features of such multicomponent nanosystems: (1) The supramolecular surface modification of BP not only can increase the stability of BP but also provides sites for further functionalization. (2) CA is a promising reactive oxygen species (ROS)-generator to boost endogenous H_2O_2 level in cancer cells, and Fc is a typical CDT catalyst. The integration of CA and Fc into a molecular structure could synchronously elevate H_2O_2 level and catalytic iron amount in acidic tumor microenvironment, which could realize self-amplified Fenton reaction for CDT. (3) The host-guest pair of cyclodextrin and Fc was used as a stimulus-responsive site because of its redox-responses, which enable the assembly to undergo rapid dissociation in the presence of endogenous H_2O_2 accompanied by the release of hydroxyl radicals [49]. (4) HA as a polysaccharide with good water solubility, biocompatibility, and targeting effect, and the HA unit not only serve as a hydrophilic biocompatible outer shell to improve stability and biocompatibility of assembly, but also ensure minimize side effects and achieve the tumor-specific therapy [50,51].

BP nanosheets were prepared by basic solvent exfoliation from bulk BP, and the morphology was characterized by transmission electron microscopy (TEM) (Fig. S1a in Supporting information). The size of BP nanosheets was 100–200 nm, which was in accordance with that measured from dynamic light scattering (DLS) analysis (Fig. S2a in Supporting information). Benefiting from the positively charged guanidinium moiety, BP@Guano-CD were prepared by the supramolecular surface modification of BP with Guano-CD *via* electrostatic interaction. TEM image showed that the size of BP@Guano-CD was about 200 nm, and the hydrodynamic diameter of BP@Guano-CD measured from DLS was similar to that of the BP (Figs. S1b and S2b in Supporting information). Supramolecular systems tend to form aggregates *via* self-assembly in solution, and the size of aggregate particles is close to colloidal particles. Therefore, the surface of aggregate particles will also form a zeta potential with the solution, just like colloidal particles. The successful coating of Guano-CD onto BP nanosheets was verified by zeta potential measurement. Fig. 1a presents the zeta potential of Guano-CD as 15.54 mV, and the corresponding values of BP@Guano-CD increased from −25.43 mV to −4.31 mV compared with BP nanosheets. Fourier-transform infrared (FTIR) spectra also revealed the changes in the functional groups during coating (Fig. 1b and Fig. S3 in Supporting information). Compared with that of BP, the new peak at 1637 cm^{-1} appeared in FTIR of BP@Guano-CD, which belonged to the C=N stretching vibration peak of Guano group. Moreover, the vibration peak of hydroxyl (-OH, 3350 cm^{-1}) of CD was observed. Next, the structural changes of BP@Guano-CD were characterized by Raman spectra. As shown in Fig. 1c, BP exhibits three main Raman peaks, corresponding to A_{1g} at 360.9 cm^{-1}, B_{2g} and A_{2g} at 434.9 and 462.6 cm^{-1}, respectively. The peaks

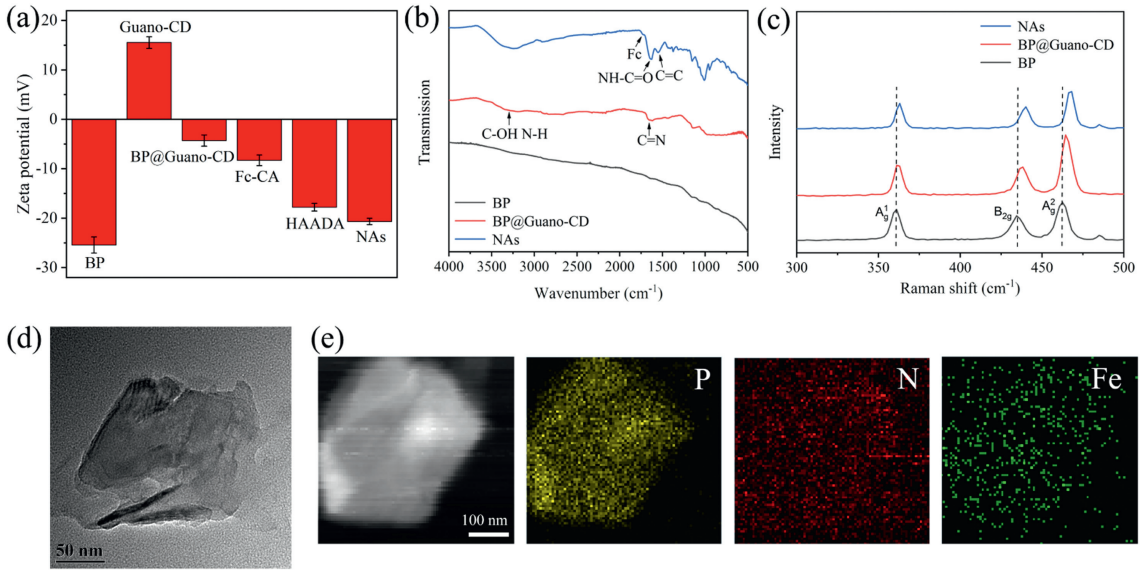

Fig. 1. Characterization of BP@Guano-CD and NAs. (a) Zeta potentials of BP, Guano-CD, BP@Guano-CD, Fc-CA, HAADA, NAs. (b) FTIR spectra and (c) Raman spectra of BP, BP@Guano-CD and NAs. (d) TEM image and (e) STEM and elemental distribution of NAs mapped by EDX.

of BP@Guano-CD are slightly red-shifted by about 1.2, 2.9, and 2.4 cm^{-1}, respectively, probably because that the surface modification of BP inhibited the vibration of surface P atoms to reduce the corresponding Raman scattering energy. These results proved the successful coating of positively charged Guano-CD onto the negatively charged BP through electrostatic interactions.

After the successful preparation of BP@Guano-CD, the multiple nanosupramolecular assembly NAs were prepared by anchoring Fc-CA and HAADA on BP@Guano-CD *via* host-guest interactions. First, the complexation behavior of Guano-CD with Fc-CA and Guano-CD with HAADA were evaluated with ^{1}H NOESY spectrum. As shown in Fig. S3a, the clear correlation peaks of the protons of Fc with the interior protons of β-CD appeared in the ^{1}H NOESY spectrum of Guano-CD with Fc-CA. The ^{1}H NOESY spectrum of Guano-CD with HAADA (Fig. S3b) also exhibited the correlation peaks of the protons of ADA with the interior protons of β-CD. These results demonstrated that the Fc and ADA moiety were efficiently embedded into the cavity of β-CD *via* host-guest interactions. Then zeta potential was performed, as shown in Fig. 1a, compared to BP@Guano-CD, the zeta potential of the resulting NAs decreased to −20.68 mV, which proved the successful combination of BP@Guano-CD, Fc-CA, and HAADA. The FTIR spectra (Fig. 1b and Fig. S4 in Supporting information) further confirmed the preparation of NAs. Compared with the spectra of BP and BP@Guano-CD, all the characteristic peaks of NAs appeared as C=N (Guano-CD) at 1637 cm^{-1}, Fe at 1729 cm^{-1}, C=C at 1542 cm^{-1} (Fc-CA) and NH–C=O (Fc-CA and HAADA) at 1638 cm^{-1}. The successful construction was also demonstrated by UV–vis spectra (Fig. S5 in Supporting information). An obvious peak appeared at 310 nm for NAs, assigned to the adsorption of Fc-CA, which further verified the combination of BP@CD and Fc-CA. The structural and morphological information come from Raman spectra and TEM. In Fig. 1c, the Raman spectra of NAs exhibit nearly identical peaks at 360.7, 437.3, and 465.9 cm^{-1} corresponding to A_{1g}, B_{2g}, and A_{2g} modes, respectively, demonstrating that the BP nanosheets with supramolecular modification did not affect the structure of the corresponding counterpart. Compared with BP@Guano-CD, TEM image showed that the average size of NAs was about 200 nm (Fig. 1d). The hydrodynamic diameter of NAs measured from dynamic light scattering (DLS) analysis was around 230 nm, which was suitable for efficient accumulation in tumor sites (Fig. S2c in Supporting information). The corresponding energy-dispersive X-ray spectroscopy (EDX) analysis showed the elemental composition (Fig. 1e), further confirming the successful construction of NAs based on the host–guest complexation interactions.

Subsequently, the photothermal properties of NAs were evaluated by examining the changes in temperature upon irradiation by near-infrared light. BP and NAs in different concentrations were irradiated with an 808 nm near-infrared laser (1 W/cm^2) for 10 min, and the real-time temperature change was recorded with an infrared thermal imager (Fig. 2a). As shown in Figs. 2b and c, both bare BP and NAs showed a clear concentration-dependent temperature evaluation. As expected, the photothermal properties of NAs was comparable to that of bare BP, both the temperature can remarkably reach 44.9 °C after irradiation for 10 min at a relatively low BP concentration (containing 100 μg/mL BP nanosheets). Moreover, the NAs also exhibited laser-power-dependent photothermal property (Fig. 2d). These results confirmed that the supramolecular surface modification of BP exhibited negligible influence on the photothermal properties of BP nanosheets. Subsequently, the stability of the NAs was evaluated. As shown in Fig. 2e, after irradiation with 808 nm NIR laser (1 W/cm^2) for 5 cycles, there was no obvious change in temperature during the cycling process, suggesting satisfactory photostability. In addition, NAs also exhibited excellent stability in aqueous solution for 7 days (Fig. S6 in Supporting information).

Next, the pH sensitivity of the supramolecular polysaccharide assemblies NAs was investigated because of the acid-labile hydrazone bond in Fc-CA. Firstly, the pH-triggered release of CA from Fc-CA at pH 5.7 was detected by peak intensity integration using HPLC. As shown in Fig. S7 (Supporting information), free CA displayed a monodispersed peak at retention time of 5.5 min. As expected, the peak intensity of CA increased gradually with time when the Fc-CA was incubated at pH 5.7, which confirmed the favorable pH-responsiveness of Fc-CA. Then, the pH-responsive CA release behavior of NAs assembly was investigated at pH 5.7 and 7.2. 10.4% of CA was released from NAs at pH 7.2 over a 72 h period, whereas the corresponding value increased to 74.9% at pH 5.7 (Fig. S8 in Supporting information). That is the release rate of CA at pH 5.7 (the endosomal pH of cancer cells) was significantly higher than that at pH 7.2 (physiological pH). This result indicated that the pH-responsive property of NAs could be ascribed to the

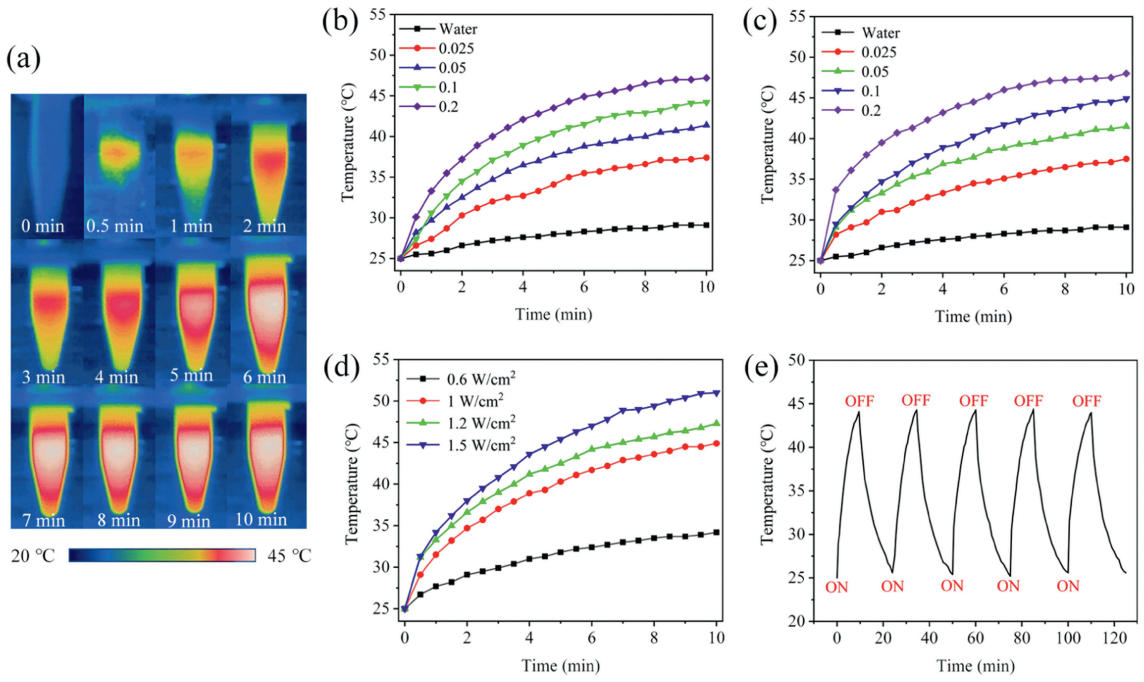

Fig. 2. (a) Real-time infrared thermal images of NAs under 808 nm NIR laser (1 W/cm^2) irradiation for 10 min. Photothermal heating curves of (b) BP and (c) NAs at different BP concentrations under 808 nm laser irradiation. (d) Photothermal heating curves of NAs under 808 nm NIR laser irradiation with different power density. (e) Photothermal stability of NAs for five on/off irradiation cycles with an 808 nm NIR laser.

acid-activated cleavage of hydrazone bond in Fc-CA. That is, NAs would release free CA under acidic condition as a first step, and then free CA undergoes a redox cycle to generate a large amount of ROS and amplify H_2O_2 level for further enhanced therapeutic effect.

Subsequently, the ROS generation performance of NAs was investigated by methylene blue (MB) degradation experiments. MB is usually used as a probe to assess the Fenton reaction because its absorbance decreased accompanied by its decomposition by the generated hydroxyl radical. As displayed in Fig. 3a, in the presence of H_2O_2, NAs could lead a significant decrease in the absorbance of MB at 664 nm in aqueous solution, while no apparent changes in the absorbance was observed for MB solutions cultured with H_2O_2 or NAs alone, revealing the degradation of MB by the hydroxyl radical generated *via* a Fenton-like reaction between H_2O_2 and NAs, indicating that this NAs could release hydroxyl radicals upon exposure to H_2O_2 for potential CDT. Considering the pH-responsive release of CA, the hydroxyl radical production capacity of NAs in acidic conditions were further evaluated, and the result showed that the MB degradation efficacy was significantly increased, that means the catalytic efficacy of Fenton reaction would be enhanced at acidic pH value with the assistance of free CA. Furthermore, given that BP could produce enormous amounts of ROS when irradiated with an 808 nm laser, the MB degradation experiment was further investigated under 808 nm laser irradiation. As we expect, the degradation of MB could be accelerated with NIR irradiation, such as the MB degradation efficacy increased from 52.79% to 88.43% within 20 min (Fig. 3b). Moreover, the H_2O_2 and BP dose-dependent degradation experiments were evaluated (Figs. 3c and d). The degradation rates of MB increased with the increase in H_2O_2 or BP dose, indicating more sufficient $^{\bullet}OH$ generation. In addition, after undergoing Fenton reaction, the hydrophobic Fc moieties were oxidized into hydrophilic charged Fc^+, which could come out of the cavity of CD, causing the rapid dissociation of NAs. These results indicated that this multiple nanosupramolecular assembly NAs could ensure satisfactory CDT efficiency, which could be developed to combine with photothermal therapy for synergistic therapy.

The generation of hydroxyl radicals in mouse 4T1 breast cancer cells by NAs was evaluated *via* fluorescent confocal image experiments by using the intracellular ROS probe 2′,7′-dichlorofluorescin diacetate (DCFH-DA), which could be oxidized by ROS to generate green fluorescence. As shown in Fig. 4a, no green fluorescence was observed in the cells incubated with PBS. In contrast, the cells incubated with NAs exhibited intense green fluorescence, indicating that the ROS level increased by efficient Fenton reaction catalyzed by Fc moiety of NAs. Importantly, the cells incubated with NAs with 808 nm laser irradiation showed enhanced green fluorescence than without NIR group, indicating that NIR could promote the ROS generation, which was consistent with the results of MB degradation experiments.

Benefiting from the good photothermal performance and effective ROS generation, NAs was utilized for combined PTT and CDT applications. Then the cytotoxicity of the NAs was investigated by measuring the relative cellular viability of cancer cells (4T1 cells and A549 human lung cancer cells) over-expressing the HA receptors, and normal cells (L929 mouse fibroblasts cells) through CCK-8 assay. As shown in Fig. 4b, NAs exhibited negligible cytotoxicity to L929 cells in the absence of NIR irradiation due to the satisfactory biocompatibility of the building blocks. As expected, NAs exhibited a dose-dependent cytotoxicity against 4T1 cells and A549 cells without NIR laser irradiation (Figs. 4c and d). This could be attributed to the self-amplified Fenton reaction of NAs and thereafter the generation of ROS within tumor cells. Besides, it could be clearly observed that the cell viability of NAs in the 4T1 cells and A549 cells were lower than that in the L929 cells. This result was attributed to the HA-enhanced targeted delivery towards 4T1 cells and A549 cells that over-express HA receptors on their surface, thus achieving targeted delivery through receptor-ligand binding and pH-responsive cascaded Fenton reaction. Furthermore, after irradiation, NAs showed much higher cytotoxicity toward 4T1 cells and A549 cells at the equivalent concentrations of NAs with-

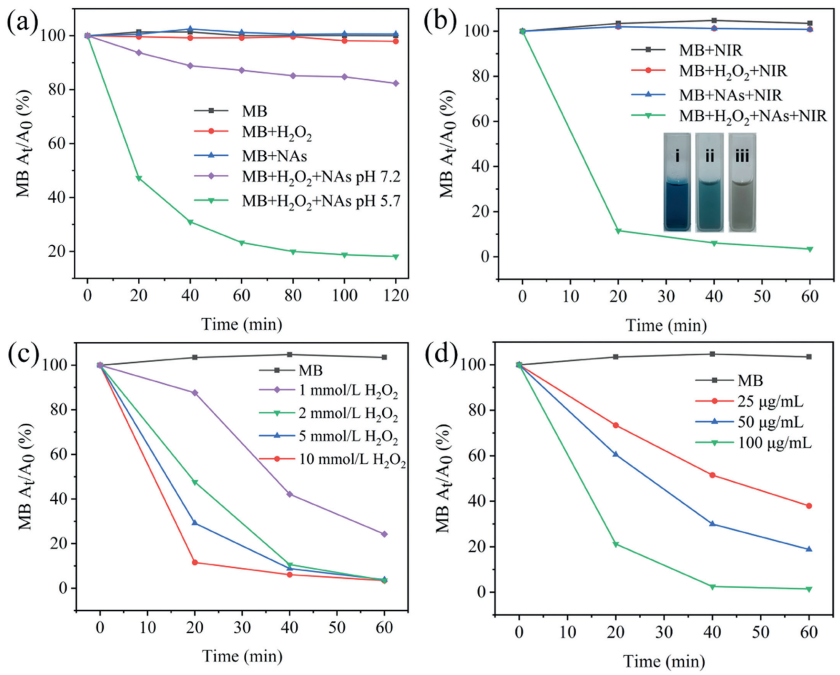

Fig. 3. Characterization of the ·OH production capacity of NAs. (a) Time-dependent degradation of MB caused by ·OH generated from NAs in the presence or absence of H_2O_2 (10 mmol/L) at pH 5.7 and 7.2. (b) MB degradation by ·OH generated from NAs in the presence or absence of H_2O_2 (10 mmol/L) at pH 5.7 with 808 nm NIR laser (1 W/cm^2) irradiation. Insert: Photographs of MB + NAs +H_2O_2: (i) at 0 min, (ii) at 120 min, (iii) at 60 min with NIR irradiation. (c) MB degradation by ·OH generated from NAs with different concentrations of H_2O_2 (1, 2, 5, 10 mmol/L) at pH 5.7 with 808 nm NIR laser (1 W/cm^2) irradiation. (d) MB degradation by ·OH generated from NAs at different concentration of BP (25, 50, 100 μg/mL) with H_2O_2 (10 mmol/L) at pH 5.7 under 808 nm NIR laser (1 W/cm^2) irradiation.

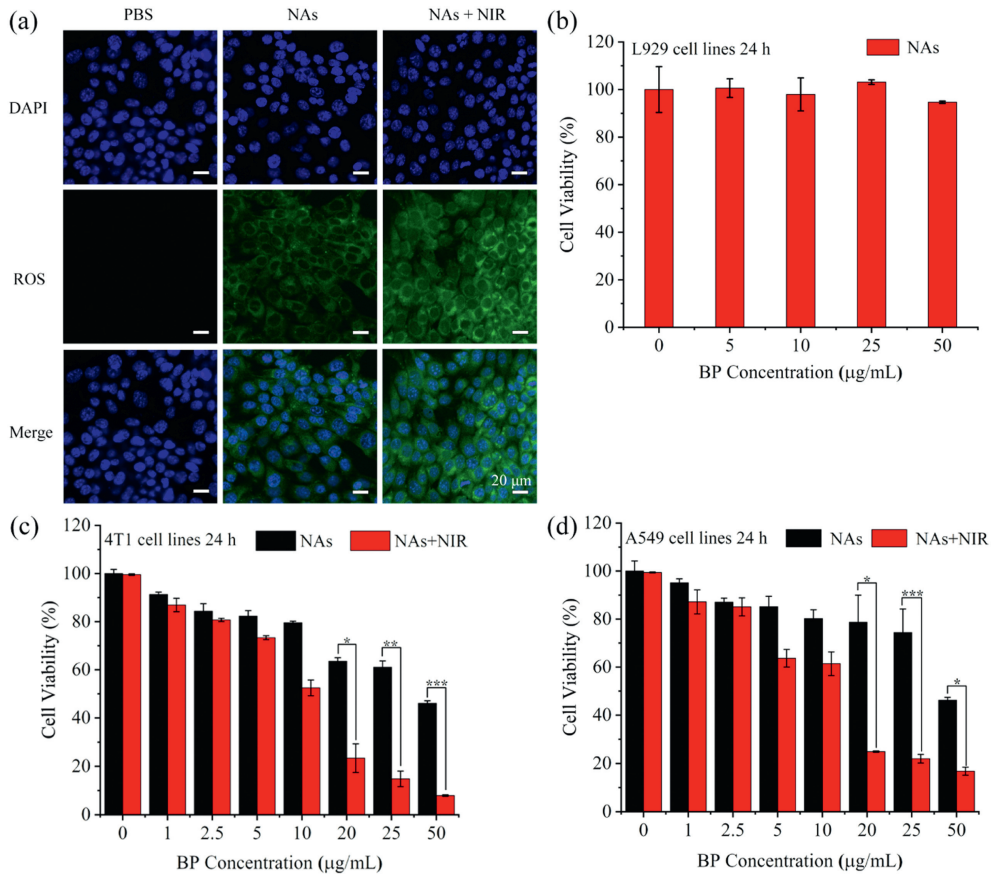

Fig. 4. (a) CLSM images of detection of intracellular ROS generation in 4T1 cells by DCFH-DA. (b) Relative viabilities of L929 cells after treated with NAs at different BP concentrations. (c) 4T1 cells and (d) A549 cells after treated with NAs at different BP concentrations without or with 808 nm NIR laser (NIR, 1 W/cm^2) irradiation for 10 min ($^*P < 0.05$, $^{**}P < 0.01$, $^{***}P < 0.001$).

out NIR irradiation, which confirmed the photothermal cytotoxicity of NAs. This result also indicated that NAs exhibited synergistic targeted photothermal and chemodynamic cytotoxic towards tumor cells.

In conclusion, black phosphorous-based pH/redox dual-responsive noncovalent multiple nanosupramolecular assembly NAs were successfully constructed for targeted photothermal and chemodynamic synergistic therapy. The sequential deposition of Guano-CD, Fc-CA, and HAADA onto the BP was achieved by cooperative electrostatic and host-guest interactions. In the presence of overproduced endogenous H_2O_2 and acidic lysosome environments of tumor cells, the NAs could be dissociated to release CA and simultaneously achieve enhanced Fenton reaction for synergistic chemodynamic/photothermal therapy. This drug delivery system displayed a synergistic effect in suppressing cancer cell proliferation and no obvious toxicity towards normal cells. Such a BP NS-based platform holds great potential as PTT-based combinational therapy platform.

Declaration of competing interest

The authors declare that they have no known competing financial interests or personal relationships that could have appeared to influence the work reported in this paper.

CRediT authorship contribution statement

Yu-Hui Zhang: Writing – review & editing, Supervision, Funding acquisition, Formal analysis. **Ye Tian:** Investigation. **Xianliang Sheng:** Methodology, Conceptualization. **Chen-Shuang Liu:** Investigation. **Lu-Qiang Wei:** Software. **Jie Wang:** Formal analysis, Conceptualization. **Yong Chen:** Writing – review & editing, Supervision, Conceptualization.

Acknowledgments

This work was supported by the Program for improving the Scientific Research Ability of Youth Teachers of Inner Mongolia Agricultural University (No. BR220140), the National Natural Science Foundation of China (No. 52263013), the Natural Science Foundation of Inner Mongolia Autonomous Region (No. 2021MS02023), the Grassland Talents program of Inner Mongolia Autonomous Region, and the Program of Higher-level Talents of Inner Mongolia Agricultural University (No. NDGCC2016-21).

Supplementary materials

Supplementary material associated with this article can be found, in the online version, at doi:10.1016/j.cclet.2024.110193.

References

[1] W. Zhou, T. Pan, H. Cui, et al., Angew. Chem. Int. Ed. 58 (2019) 769–774.
[2] L. Sutrisno, H. Chen, Y. Chen, et al., Biomaterials 275 (2021) 120923.
[3] Z. Li, J. Song, H. Yang, Sci. China Chem. 66 (2023) 406–435.
[4] L. Chan, X. Chen, P. Gao, et al., ACS Nano 15 (2021) 3047–3060.
[5] X. Bai, R. Wang, X. Hu, et al., ACS Nano 18 (2024) 3553–3574.
[6] J. Huang, B. He, Z. Zhang, et al., Adv. Mater. 32 (2020) 2003382.
[7] L. Deng, Y. Xu, C. Sun, et al., Sci. Bull. 63 (2018) 917–924.
[8] J. Long, Z. Yao, W. Zhang, et al., Adv. Sci. 10 (2023) 2302539.
[9] Y. Zhao, L. Tong, Z. Li, et al., Chem. Mater. 29 (2017) 7131–7139.
[10] Y. Xu, X. Li, Y. Song, et al., ACS Appl. Mater. Interfaces 13 (2021) 50270–50280.
[11] Q. Zhou, Q. Chen, Y. Tong, J. Wang, Angew. Chem. Int. Ed. 55 (2016) 11437–11441.
[12] G. Liu, H.I. Tsai, X. Zeng, et al., Chem. Eng. J. 375 (2019) 121917.
[13] K. Hu, L. Xie, Y. Zhang, et al., Nat. Commun. 11 (2020) 2778.
[14] X. Zeng, M. Luo, G. Liu, et al., Adv. Sci. 5 (2018) 1800510.
[15] W. Liu, A. Dong, B. Wang, H. Zhang, Adv. Sci. 8 (2021) 2003033.
[16] X. Zhang, Z. Zhang, S. Zhang, et al., Small 13 (2017) 1701210.
[17] J. Zuo, X. Gao, J. Xiao, Y. Cheng, Chin. Chem. Lett. 34 (2023) 107827.
[18] S. Bai, Y.F. Han, Acc. Chem. Res. 56 (2023) 1213–1227.
[19] C. Liu, H. Bu, X. Duan, H. Li, Y. Bai, ACS Appl. Mater. Interfaces 15 (2023) 38264–38272.
[20] D. Wu, Z. Zhang, X. Li, et al., Biomacromolecules 24 (2023) 1022–1031.
[21] M.X. Wu, H.J. Yan, J. Gao, et al., ACS Appl. Mater. Interfaces 10 (2018) 34655–34663.
[22] M. Zuo, W. Qian, K. Wang, L. Wang, X.Y. Hu, Mater. Chem. Front. 6 (2022) 2790–2795.
[23] C. Zhang, J. Niu, J. Li, et al., Chin. Chem. Lett. 35 (2024) 108556.
[24] X. Zhu, J.X. Wang, L.Y. Niu, Q.Z. Yang, Chem. Mater. 31 (2019) 3573–3581.
[25] T. Xiao, X. Li, L. Zhang, et al., Chin. Chem. Lett. 35 (2024) 108618.
[26] G. Li, Z. Zhuo, B. Wang, et al., J. Am. Chem. Soc. 143 (2021) 10920–10929.
[27] J. Yang, C. Fang, H. Liu, et al., Nanoscale 13 (2021) 15085–15099.
[28] J. He, G. Chen, P. Zhao, C. Ou, Nano Res. 14 (2021) 3988–3998.
[29] H. Wang, Y. Li, H. Yu, et al., J. Am. Chem. Soc. 141 (2019) 13187–13195.
[30] Z. Xu, S. Jia, W. Wang, et al., Nat. Chem. 11 (2019) 86–93.
[31] L. Peng, S. Liu, A. Feng, J. Yuan, Mol. Pharmaceutics 14 (2017) 2475–2486.
[32] Y. Wang, B. Ma, A.A. Abdeen, et al., ACS Appl. Mater. Interfaces 10 (2018) 31915–31927.
[33] Y. Wang, Z. Pei, W. Feng, Y. Pei, J. Mater. Chem. B 7 (2019) 7656–7675.
[34] Y. Bai, C.P. Liu, F.Y. Xie, et al., Carbohyd. Polym. 213 (2019) 411–418.
[35] H. Wang, P. Liang, L. Zhang, et al., Chin. Chem. Lett. 34 (2023) 108129.
[36] T. Ji, S. Li, Y. Zhang, et al., ACS Appl. Mater. Interfaces 8 (2016) 3438–3445.
[37] Y.M. Zhang, N.Y. Zhang, K. Xiao, Q. Yu, Y. Liu, Angew. Chem. Int. Ed. 57 (2018) 8649–8653.
[38] W. Zhang, Z. Zheng, L. Lin, et al., Adv. Sci. 10 (2023) 2304062.
[39] W. Zhang, L. Lin, J. Guo, et al., Research 2022 (2022) 9814638.
[40] Y.H. Zhang, C.S. Liu, Y. Tian, et al., Int. J. Biol. Macromol. 242 (2023) 125194.
[41] J. Tian, B. Huang, Z. Cui, et al., Acta Biomater. 130 (2021) 447–459.
[42] H. Yang, Z. Duan, F. Liu, Z. Zhao, S. Liu, ACS Macro Lett. 12 (2023) 295–301.
[43] W. Zhang, P. Xiao, L. Lin, et al., Chin. Chem. Lett. 33 (2022) 4043–4047.
[44] Y. Ding, C. Wang, Y. Ma, et al., Acta Biomater. 143 (2022) 381–391.
[45] B.Y. Liu, X.L. Yang, X. Xing, et al., ACS Macro Lett. 8 (2019) 719–723.
[46] Z. Li, Y.M. Zhang, H.Y. Wang, H. Li, Y. Liu, Macromolecules 50 (2017) 1141–1146.
[47] X. Xu, Z. Zeng, J. Chen, et al., Chem. Eng. J. 390 (2020) 124628.
[48] Y. Zhang, L. Wang, J. Wang, S. Xin, X. Sheng, Chin. Chem. Lett. 32 (2021) 1902–1906.
[49] K. Yang, G. Yu, Z. Yang, et al., Angew. Chem. Int. Ed. 60 (2021) 17570–17578.
[50] X. Hou, D. Zhong, H. Chen, et al., Carbohyd. Polym. 292 (2022) 119662.
[51] J. Shinn, S. Park, S. Lee, et al., ACS Nano 18 (2024) 4704–4716.